Aggregation of an Amphiphilic Poly(*p*-phenylene) in Micellar Surfactant Solutions. Static and Dynamic Light Scattering

Tobias Fütterer, Thomas Hellweg,* and Gerhard H. Findenegg

Stranski-Laboratorium für Physikalische und Theoretische Chemie, Technische Universität Berlin, Strasse des 17.Juni 112, D-10623 Berlin, Germany

Jörg Frahn and A. Dieter Schlüter

Institut für Chemie/Organische Chemie, Freie Universität Berlin, Takustr. 3, D-14195 Berlin, Germany

Received February 14, 2005; Revised Manuscript Received June 20, 2005

ABSTRACT: The aggregation of a short-chain nonionic amphiphilic poly(*p*-phenylene) in aqueous micellar solutions of the nonionic surfactants C_8E_4, $C_{12}E_6$, or $C_{10}G_2$ was studied. Cryo-transmission electron microscopy reveals the existence of fiberlike aggregates of mean length greater 200 nm and a diameter of ca. 6 nm surrounded by an excess of small surfactant micelles in these solutions. Static and dynamic light scattering were used to characterize the fiber aggregates in these complex liquid mixtures. The scattering data were analyzed by model-based and model-independent procedures, which yield the mean length L, the polydispersity k, and the radial aggregation number N_{rad} of the fiber aggregates. The dynamic behavior of the aggregates can be described by a model for polydisperse rigid rods, taking into account their translational and rotational diffusion.

I. Introduction

Poly(*p*-phenylene)s (abbreviated as PPP) are intrinsically stiff linear molecules. Applications of these and similar backbone polymers in photo- and electroluminescent devices arise from their peculiar electronic structure.[1−6] In this work we study the aggregation of an amphiphilically substituted nonionic PPP oligomer, in which each benzene ring of the aromatic backbone is substituted with an alkyl chain ($-C_{12}H_{25}$) and an oxyethylene chain ($-CH_2(OC_2H_4)_3OMe$) in the para position to the alkyl substituent (see Figure 1). This amphiphilic substitution scheme generates a boundary between the hydrophilic and hydrophobic substituents in a plane parallel to the major axis of the PPP. Amphiphilically substituted PPPs represent a relatively new class of materials. Their structure suggests an interesting self-assembly behavior, but to our knowledge only a few systems have been studied at present (e.g., refs 7−10).

One remarkable example of such backbone polymers is PPP-sulfonate polyelectrolyte studied by Bockstaller et al.[11,12] In aqueous solutions these molecules form elongated cylindrical aggregates of constant diameter but variable length, depending on the molar mass of the PPP-sulfonates. This behavior indicates a lengthwise aggregation of these macromolecules. The cylindrical aggregates of mean length $L \approx 280$ nm and diameter $d = 3.4$ nm formed by a PPP-sulfonate with an average number of $n \approx 100$ benzene rings in the backbone were found to form the building blocks for a higher level of ordered supramolecular structures. At polymer concentrations of ca. $c = 0.1$ g/kg clusters of cylindrical aggregates with internal lyotropic ordering are formed; above a concentration $c_{crit} = 1.1$ g/kg a nematic phase is observed. The critical concentration for the formation of a nematic phase, $c_{crit} = 1.1$ g/kg, is significantly below

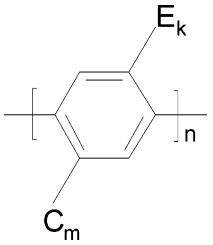

Figure 1. Poly(*p*-phenylene) oligomer PPP(12): $C_m = -C_{12}H_{25}$, $E_k = -CH_2(OC_2H_4)_3OMe$ with $n \approx 12$.

$c_{nemat} = 12$ g/kg predicted by the Onsager theory[13] for uncharged cylindrical aggregates of the same length L and diameter d. This is explained with a counterion condensation theory for univalent counterions.[11,12]

The present PPP is uncharged and has a smaller number of benzene rings along the backbone compared to the PPP-sulfonates investigated by Bockstaller et al. It was of interest to find out whether the present polymer exhibits lengthwise aggregation in the same way as the charged PPP-sulfonates. The dependence of the mean length of such cylindrical PPP aggregates on the polymer concentration has not been investigated yet. Thermodynamic models[14] and mean-field theories[15] of reversible chain aggregation ("living polymers") predict a dependence as $L \propto c^{\alpha}$, with $\alpha = 0.5$, as was indeed found for wormlike micelles of e.g. $C_{12}E_5$ in H_2O.[16] Therefore, in the present study we are going to investigate the scaling behavior of L with respect to concentration. Furthermore, one expects that the interactions between the cylindrical aggregates of the present PPP should be different from those studied by Bockstaller et al. since they are not dominated by Coulomb interactions. If supramolecular structures, such as clusters of cylindrical aggregates or a nematic phase, can be observed for the present molecules, the critical concentration for the uncharged stiff cylinders should be shifted to higher values compared to the charged PPP-sulfonate aggregates according to the Onsager theory.[13]

* To whom correspondence should be addressed. E-mail thomas.hellweg@tu-berlin.de.

10.1021/ma050318h CCC: $30.25
Published on Web 07/26/2005

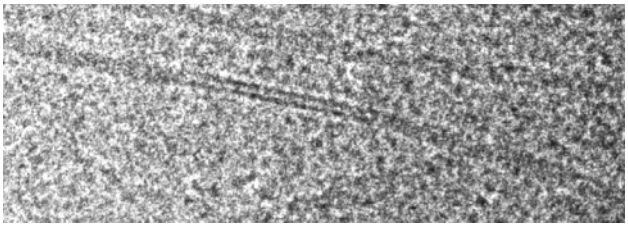

Figure 2. Cryo-TEM image of PPP(12) in a micellar solution of the surfactant C_8E_4. The elongated objects represent fiber aggregates and the small objects represent surfactant micelles. The width of this image is equivalent to 180 nm (from ref 21).

The pure polymer PPP(12) is almost insoluble in water, but it can be solubilized in aqueous surfactant solutions. Nonionic surfactants of the alkyl poly(oxyethylene) type, C_iE_j,[17,18] and alkyl poly(glucoside) type, C_iG_j,[19,20] were used in this work. Cryogenic transmission electron microscopy (cryo-TEM) reveals that PPP(12) forms elongated fiberlike aggregates of a contour length $L > 200$ nm and a diameter $d = 5.9$ nm in the presence of excess surfactant micelles (see Figure 2 and ref 21). The observed aggregates seem to be remarkably stiff.

Colloidal systems often contain two or more types of particles of different size and shape. For example, several surfactant systems are known to contain vesicles coexisting with compact spherical micelles in a certain concentration range.[22,23] Aqueous solutions of diblock copolymers may contain spherical and wormlike chain aggregates at the same time.[24,25] Scattering techniques with light, X-rays, and neutrons are most frequently used for an in-situ characterization of colloidal dispersions. However, the determination of the properties of one specific type of particle in such complex systems is a challenge for the analysis of the scattering data.

In this study we have adopted a model-based analysis of dynamic and static light scattering (DLS, SLS) data of the PPP aggregates in water, based on results of the cryo-TEM images. The DLS data analysis includes a model for polydisperse rigid rods and yields the mean length L and the polydispersity parameter k of the fiber aggregates. The combined analysis of the DLS and SLS data of this complex liquid based on a form factor model yields the molar mass M_w and the radial aggregation number N_{rad} of the fiber aggregates. The determination of the surfactant distribution inside the aggregates and the determination of the diameter of the aggregates by means of small-angle neutron scattering will be described in a second publication on this subject.[26]

II. Samples and Experimental Setup

A. Materials. The polymer PPP(12) studied in this work was synthesized by the transition-metal-catalyzed Suzuki step-growth polymerization technique described elsewhere.[27−29] The sample was characterized by gel permeation chromatography (GPC) which yielded a number- and mass-average molar mass of $M_n = 5200$ g/mol ($n_n = 12$) and $M_w = 8700$ g/mol ($n_w = 21$), corresponding to a ratio $M_w/M_n = 1.7$.

The surfactant tetra(oxyethylene)monooctyl ether (C_8E_4) was purchased from Nikko Chemicals Co., Japan (>99% purity). The surfactant hexa(oxyethylene)monododecyl ether ($C_{12}E_6$) was purchased from Nikko Chemicals Co., Japan (>99% purity). The surfactant decyl-β-glucosid ($C_{10}G_2$) was purchased from Calbiochem, Bad Soden, Germany (>99% purity).

High-purity water from a Milli-Q water purification system (Millipore/Waters) was used for all light scattering experiments.

Table 1. Concentrations of PPP(12) and C_8E_4 in H_2O for the Light Scattering Investigations: Series H with Constant Concentration Ratio and Series K with Constant Surfactant Concentration[a]

	c_{PPP} [wt %]	$c_{C_8E_4}$ [wt %]	c_{m,C_8E_4} [wt %]
series H			
1	0.052	0.49	0.27
2	0.10	0.98	0.76
3	0.21	1.95	1.73
4	0.41	3.91	3.69
series K			
1	0.050	1.98	1.76
2	0.077	1.98	1.76
3	0.101	1.98	1.76
4	0.307	1.98	1.76
5	0.410	1.98	1.76

[a] A value of $cmc_{C_8E_4} = 0.2176$ wt % for the critical micellar concentration of C_8E_4 is used to calculate c_m.

B. Sample Preparation. Solutions of the polymer PPP-(12) in aqueous media were prepared by adding 0.05−0.4 wt % of the polymer to 0.5−4 wt % micellar solutions of the surfactants C_8E_4, $C_{12}E_6$, or $C_{10}G_2$ in water. The pure surfactant solutions were filtered (pore size 200 nm; Schleicher & Schuell) directly into the sample cells (quartz, Hellma, Germany); after addition of the polymer the mixtures are treated in an ultrasonic bath (35 kHz) for at least 2 h at ca. 45 °C. At this elevated temperature the aqueous systems are phase separated into a surfactant-rich and a dilute aqueous phase. After remixing and equilibration at room temperature the solutions were investigated without further filtering to avoid concentration changes of the samples.

Determination of the length L of the fiber aggregates on the concentration of PPP(12) was performed with C_8E_4 as the surfactant in two independent series, denoted as H and K. Four solutions with constant ratio of the PPP to surfactant concentration and five solutions with constant surfactant and increasing PPP concentration were prepared. The respective concentrations are listed in Table 1. At lower ratios of $c_{m,C8E4}/c_{PPP} \approx 5$ it was not possible to dissolve all of the polymer. Because of this it was not possible to prepare samples without an excess of pure surfactant micelles. Samples with higher concentrations of polymer as 0.6 wt % PPP(12) were not prepared due to the limited amount of polymer available.

C. Static and Dynamic Light Scattering. LS measurements were performed using commercial equipment for simultaneous static and dynamic experiments from ALV-Laservertriebsgesellschaft (Langen, Germany). The light source employed was the blue line ($\lambda = 488$ nm) of a Coherent argon ion laser (Innova 90), operating with a constant output power of ≈150 mW. For the DLS experiments an ALV-5000 multiple τ hard wire correlator (256 channels, first lag time 200 ns) was used. Details about the experimental setup for the light scattering are given elsewhere.[25,30] The scattering experiments were performed in an angular range $30° > \theta > 150°$, resulting in a q range of $0.008\ 88\ nm^{-1} < q < 0.033\ 18\ nm^{-1}$. The static light scattering (integrated) intensity was normalized to the primary beam intensity and brought to absolute scale using a toluene reference for calibration.[31] All LS measurements were performed in the VV geometry. The refractive index increment dn/dc was measured with a commercial refractometer (DB1/b, Baur Electronics, Germany) at $\lambda = 488$ nm.

III. Theory, Data Analysis, and Results

A. Dynamic Light Scattering. A detailed description of the theoretical background for dynamic light scattering data analysis can be found in ref 32. In the present system we have to deal with at least two different types of particles: fiberlike polymer aggregates and surfactant micelles (see Figure 2). The analysis of the field autocorrelation function $g_1(\tau)$ by an inverse Laplace transformation (CONTIN, 100 grid points)[33,34] did not yield a consistent picture of the dynamic

behavior of the system. This analysis resulted in one, two, or three separated contributions to the relaxation rate distribution function $G(\Gamma)$. The number of resolved contributions, their mean relaxation rates Γ_i, and their width varied more or less arbitrarily with the scattering angle θ. Because of this, we applied a model-based approach to analyze the measured correlation functions.

On the basis of the observation of two different species on the cryo-TEM micrographs, small spherical micelles, and stiff elongated fiber aggregates, we applied a sum of an exponential decay function to account for the small micelles and of a dynamic model to describe the behavior of the PPP fibers. Also, this approach does not yield a satisfactory data description. Even if extremely broad length distribution functions for the fiber aggregates are considered, this model still leads to high deviations from the measured data. In addition, the resulting relaxation times correspond to very high values for the fiber length, $L_n \gg 1500$ nm. These lengths would result in the formation of a nematic phase order in the system. But even for the highest PPP(12) concentration no birefringence and hence no such ordering is observed. Additionally, the cryo-TEM micrographs indicate a significantly shorter average length L_n compared to the outcome of this approach. To achieve a satisfactory representation of the experimental data for the observed q range, a third contribution with a small diffusion coefficient had to be considered. The origin of this third contribution to the dynamic behavior of this complex liquid is denoted as "cluster contribution" in the following (see the respective section for a more detailed discussion). The crucial point in our model-based analysis is the simultaneous fit of four correlation functions measured at different scattering angles θ. The simultaneous fit implies a specific q dependence for the relaxation rates of the three contributions, and thus, the information on the Γ_i gained at one angle is used to describe the correlation function at another angle in the simultaneous fit procedure. This allows for a separation of the three contributions even at a scattering angle at which CONTIN is not able to compute distinct contributions for the three types of dynamics. As the investigated q range is quite broad ($30° < \theta < 150°$) shortcomings of the used model would appear as an unsatisfactory description of the q dependence.

The measured intensity autocorrelation function $g_2(\tau)$ is related to the field autocorrelation functions $g_1(\tau)$ of the three species (small surfactant micelles, stiff fiber aggregates, and large clusters) according to the Siegert relation[32] by

$$g_2(\tau) = f^*\left(\frac{a_F g_{1,F}(\tau) + a_C g_{1,C}(\tau) + a_M g_{1,M}(\tau)}{a_F + a_C + a_M}\right)^2 + 1 \quad (1)$$

where f^* is the instrumental coherence factor and $a_i(q)$ are the amplitudes of the individual field autocorrelation functions $g_{1,i}$ (F ≡ fiber, C ≡ cluster, M ≡ micelle). In the data analysis the g_1 functions of the micelles and clusters were represented by a single-exponential decay according to

$$g_1(\tau) = \exp(-\Gamma\tau) \quad (2)$$

where $\Gamma = D_{tr}q^2$, with D_{tr} the translational diffusion coefficient[32] and the magnitude of the scattering vector q is given by $q = 4\pi \sin(\theta/2)/\lambda$, with θ the scattering angle and λ the wavelength in the medium. The normalized fiber contribution $g_1(\tau)_{fiber}$, with a polydispersity distribution for the length L according to Schulz–Zimm, is given by[35]

$$g_{1,fiber}(\tau) = \frac{\sum_L p(k,L_n,L) g_{1,fiber}(\tau,L)}{\sum_L p(k,L_n,L)} \quad (3)$$

where $p(k,L_n,L)$ is the z-average size distribution (Schulz–Zimm,[35,36] with $k = 1/(M_w/M_n - 1)$ and L_n is the number-average length of the fiber aggregates. $g_{1,fiber}(\tau,L)$ accounts for the dynamic behavior of stiff cylinders with monodisperse length L. The cylindrical particles investigated here are stiff in good approximation; i.e., the persistence length L_p is of similar magnitude as the contour length L. To deal with these fiberlike particles, we use a model of stiff rods proposed by Pecora[35–39]

$$g_{1,F}(\tau,L) = \sum_{n=0}^{10} S_n(2n,qL) \exp(-(D_{tr}q^2 + x(n)D_{rot})\tau) \quad (4)$$

with $x(n) = 4n^2 + 2n$. The translational motion is described by one averaged diffusion coefficient D_{tr} which is independent of the rotational diffusion (D_{rot}). The overall motion of the particle is determined by combinations of translation and rotation. The amplitudes S_n of the modes relate to different length scales with respect to the length L, as they depend on the product of the scattering vector q and the length L, and are proportional to the square of the integral over a spherical Bessel function of the $2n$-th order.[38] For values of $qL \leq 4$, only the pure translation (S_0) contributes to the intermediate scattering function. For values of $qL \leq 50$, the first 11 modes have to be taken into account.[38,40] Both the translational diffusion coefficient and the rotational diffusion coefficient depend on the geometry (length L, diameter d) and flexibility (L_p/L) of the rods. For rigid particles, Kirkwood and Riseman derived a relation between the diffusion coefficients and the particle geometry, based on the Oseen approximation,[41] viz.

$$D_{tr} = \frac{k_B T}{3\pi\eta_0 L}\ln\left(\frac{L}{d}\right) \quad \text{and} \quad D_{rot} = \frac{9D_{tr}}{L^2} \quad (5)$$

where k_B is the Boltzmann constant, T the temperature, and η_0 the viscosity of the solvent. The model of Broersma,[42,43] even in its corrected form, does not provide a better representation than the simple Kirkwood–Riseman approach.[38]

Fitting the model described in the previous paragraph to the experimental data leads to the average length L_n and the shape and width of the length distribution, represented by k. The parameters of the model are independent of the scattering vector q, except the amplitudes $a_i(q)$ and f^*. Hence, a parameter set for a given q must describe the dynamic behavior at other q values as well (except the amplitudes $a_i(q)$ and f^*). To implement this into the data analysis, a simultaneous fit of $g_2(\tau)$ at four different q values was performed. Free adjustable parameters in the fitting procedure were the instrumental coherence factor f^*, the mean fiber length L_n, the polydispersity k (Schulz–Zimm), the amplitude $a(q)_{cluster}$, the translational diffusion coefficient $D_{tr,cluster}$,

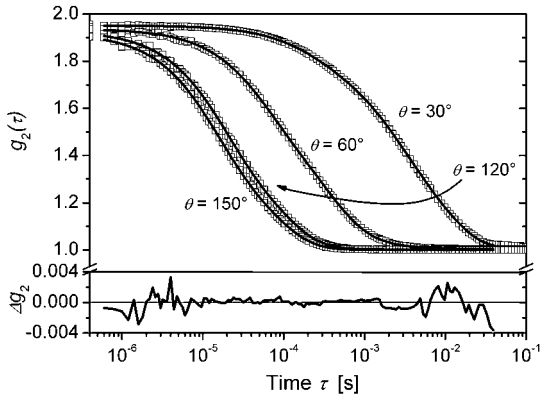

Figure 3. DLS of sample K1 (PPP(12) and C_8E_4 in H_2O) at 25 °C: Intensity autocorrelation function $g_2(\tau)$ measured at four scattering angles θ (symbols) and simultaneous fit of the four curves by eq 1 (lines). The quality of the fit is indicated by $\Delta g_2 = g_2(\tau)_{fit} - g_2(\tau)_{measur}$ at $\theta = 30°$.

the amplitude $a(q)_{micelle}$, and the translational diffusion coefficient $D_{tr,micelle}$. $a(q)_{fiber}$ is set to 1. The value for the diameter d of the fiber aggregates was estimated on the basis of the cryo-TEM micrographs, taking into account two hydration shells around the perimeter with a thickness of 0.3 nm for each water layer.[44] This leads to a value of $d = 7.1$ nm.

As an example, Figure 3 displays the measured intensity autocorrelation function $g_2(\tau)$ of sample K1 (see Table 1) and the respective simultaneous fit according to eq 1. The residuals in Figure 3 show that the model underlying eq 1 fits the data equally well in the whole q range and domain of relaxation times. The errors in the resulting amplitudes $a_i(q)$ and diffusion coefficients D amount to 3−8%, estimated by a parameter variation and χ^2 analysis.[45] The individual errors for L_n and k are in the same range, but the values of L_n obtained in the above multiparameter fit are not independent of the polydispersity parameter k. A parameter analysis shows that different combinations of L_n and k (resulting in similar length distribution functions $p(k,L_n,L)$) yield nearly equally good fits of the data. For L_n values from 400 to 850 nm and k values in a range from 1.5 to 4, χ^2 values below the limit $1.1\chi^2_{minimum}$ are obtained. The trend of an increase of L_n with increasing concentration was found for all parameter sets. However, the error of L_n is estimated to ±20%, which means that the error bars cover all observed L_n values for $k = 1.5-4$, if L_n is given for a mean k of 2.5.

The results of the data analysis of the intensity autocorrelation functions $g_2(\tau)$ of the sample series H and K are listed in Table 2.

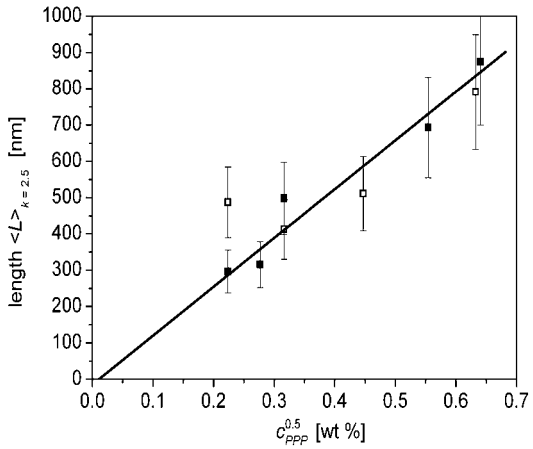

Figure 4. Dependence of the mean length L_n of the fiber aggregates on the square root of polymer concentration c_{PPP} for sample series H (open symbols) and K (full symbols): values of L_n for fixed polydispersity parameter k. The solid line represents a fit by a linear function.

Dependence of the Fiber Length on the PPP Concentration. The data analysis (Table 2) shows that the mean length L_n of the fiber aggregates increases with increasing polymer concentration c_{PPP}. For the present system the width of the length distribution, represented by k, can be assumed to be independent of the concentration c. Therefore, we use the L_n values obtained for a fixed value of k (k set to 2.5, see Table 2) to test their concentration dependence. The concentration dependence of these values of L_n is illustrated in Figure 4 for the sample series H and K. A linear fit to the L_n vs $c^{0.5}$ data is also shown in Figure 4, and the L_n values exhibit a fairly good linear relation, indicating that the concentration dependence of L_n of the fiber aggregates conforms reasonably well to the power law predicted for living polymers.

Even if the used polymer concentrations for the analysis of L_n vs $c^{0.5}$ are not correct due to the cluster formation, the linear relation of $L_n \propto c^{0.5}$ still holds since the concentration only shifts the proportionallity constant.

Cluster Contribution. We attribute the third contribution to $g_2(\tau)$ at high relaxation times to a formation of clusters by the fiber aggregates. For PPP-sulfonate polyelectrolytes Bockstaller et al.[11,12] have found a cluster formation of the fiber aggregates above mass concentrations of 0.1 g/kg in water. In the case of these charged aggregates the cluster formation is attributed to a counterion condensation. In the concentration range also investigated in the present work (c_{PPP} = 0.5−4 g/kg), Bockstaller et al. have found the formation of a

Table 2. Results for the Sample Series H and K of Simultaneous Fits of $g_2(\tau)$ Measured at Four Scattering Angles (θ_i = 30°, 60°, 120°, and 150°) with Eq 1

	fiber aggregates					clusters		micelles	
	D_{tr} [nm^2 s^{-1}]	D_{rot}	L_n [nm]	k	$L_{n,k=2.5}$ [nm]	D_{tr} [nm^2 s^{-1}]	$R_{H,0}$ [nm]	D_{tr} [nm^2 s^{-1}]	$R_{H,0}$ [nm]
series H									
1	4.25×10^6	161	560	3.88	487	7.89×10^5	311	8.22×10^7	2.98
2	4.83×10^6	256	464	3.27	412	6.45×10^5	380	6.73×10^7	3.64
3	4.10×10^6	141	423	1.64	511	6.03×10^5	407	5.95×10^7	4.12
4	2.92×10^6	42	761	2.10	791	4.34×10^5	567	5.30×10^7	4.62
series K									
1	6.18×10^6	634	308	2.58	296	6.14×10^5	399	5.89×10^7	4.16
2	5.90×10^6	535	317	2.50	315	6.72×10^5	365	5.64×10^7	4.34
3	4.18×10^6	151	479	2.31	498	5.88×10^5	417	5.81×10^7	4.22
4	3.24×10^6	61	674	2.38	693	4.37×10^5	561	5.63×10^7	4.35
5	2.70×10^6	32	653	1.15	874	3.61×10^5	679	5.82×10^7	4.21

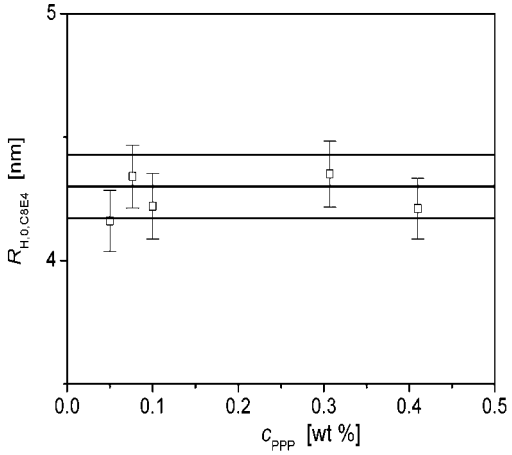

Figure 5. Hydrodynamic radius $R_{H,0,micelles}$ of C_8E_4 at 25 °C, derived from the present measurements on sample series K (open squares) and from the respective aqueous solution of C_8E_4 (straight line). The thin straight lines indicate the respective error boundaries.

nematic ordering in the aqueous solutions. Such a nematic phase was not found for the PPP system investigated here. On the basis of the Onsager theory,[13] a critical concentration c_{crit} for an isotropic−nematic transition can be estimated for uncharged stiff cylinders. For cylinders with a length of 500 nm and a diameter of 7.1 nm the concentration c_{crit} is ca. 7 g/kg. This explains why no nematic phase is observed for the present solutions. But in the investigated concentration range a cluster formation can be assumed. The found increase of the hydrodynamic radius $R_{H,cluster}$ (see Table 2) with increasing PPP concentration, i.e., with increasing length L of the aggregates, is consistent with a cluster formation. The tendency for a cluster formation increases with increasing length and increasing particle density.

Reliability of the Data Analysis. The reliability of our data analysis was tested by comparing the results for the hydrodynamic radius of the surfactant micelles, $R_{H,0}$, in a pure surfactant solution with the respective value in the presence of the polymer. Such a comparison is shown in Figure 5 for the sample series K, i.e., a micellar C_8E_4 concentration $c_{m,C8E4} = 1.76$ wt %. Values of $R_{H,0}$ were calculated from the diffusion coefficient $D_{tr,micelle}$ on the basis of the Stokes−Einstein relation, using the viscosity of pure water. The values for the mixed systems agree with those for the pure micellar system within the errors. Thus, the result of this comparison lends credibility to the data analysis of the polymer solutions. For the sample series H the found micellar hydrodynamic radius $R_{H,0,micelles}$ equals the concentration dependence of $R_{H,0,micelles}$ of the respective pure surfactant solutions.[46] This is found for the PPP(12)/$C_{12}E_6$ and PPP(12)/$C_{10}G_2$ solutions, too.

DLS on PPP(12) in $C_{12}E_6/H_2O$ and in $C_{10}G_2/H_2O$. For solutions of PPP(12) in $C_{12}E_6/H_2O$ and in $C_{10}G_2/H_2O$ the analysis of the measured intensity autocorrelation functions described above is also applied. For 0.201 wt % PPP(12) in 1.92 wt % $C_{12}E_6/H_2O$ the mean length is $L_{n,k=2.5} = 412$ nm and the hydrodynamic radius is $R_{H,cluster} = 359$ nm. The used diameter of the fiber aggregates was $d = 7.6$ nm ($d_{TEM} = 6.4$ nm and $d_{H2O} = 1.2$ nm). The found hydrodynamic radius of the pure $C_{12}E_6$ micelles in the polymer system is comparable with the respective value of a pure $C_{12}E_6/H_2O$ solution (PPP(12)/$C_{12}E_6/H_2O$: $R_{H,C_{12}E_6} = 6.65 \pm 0.14$ nm; pure aqueous surfactant solution: $R_{H,C_{12}E_6} = 6.53 \pm 0.1$ nm). For 0.18 wt % PPP(12) in 2.01 wt % $C_{10}G_2/H_2O$ the mean length is $L_{n,k=2.5} = 390$ nm and the hydrodynamic radius is $R_{H,cluster} = 338$ nm. In this case the used diameter of the fiber aggregates was $d = 7.1$ nm. The found hydrodynamic radius of the $C_{10}G_2$ micelles in the polymer system is slightly higher compared to the respective value of a pure $C_{10}G_2/H_2O$ solution (PPP(12)/$C_{10}G_2/H_2O$: $R_{H,C_{10}G_2} = 3.86 \pm 0.19$ nm; pure aqueous surfactant solution: $R_{H,C_{10}G_2} = 3.14 \pm 0.16$ nm). For both systems the found averaged length $L_{n,k=2.5}$ and $R_{H,cluster}$ are of the same order of magnitude compared to the system PPP(12) in C_8E_4/H_2O.

B. Static Light Scattering. As derived from the dynamic light scattering data analysis, the normalized static scattering intensity $R(q)$ is a sum of the three contributions. The q dependence of the amplitudes $a_i(q)$ can be expressed by the respective form factors $P(q)$ weighted with the respective amplitudes $a_i(q=0) \equiv A_i^0$ [47]

$$R(q) = A_F^0 P(q)_F + A_C^0 P(q)_C + A_M^0 P(q)_M \qquad (6)$$

with F ≡ fiber, C ≡ cluster, and M ≡ micelle. The A_i^0 are proportional to the mass concentration c_i, the contrast factor K_i, and the apparent molar mass $M_{w,i,app}$ of the respective particles

$$A_i^0 = K_i c_i M_{w,i,app} \qquad (7)$$

The contrast factor K_i is given by $K_i = 4\pi^2 n_0^2/\lambda_0^4 N_A (dn/dc)_i^2$, with the refractive index increment $(dn/dc)_i$, the wavelength λ_0, and the refractive index of the solvent n_0.

The static model must be capable to describe the q dependence measured in a static light scattering experiment as well as the q dependence of the amplitudes $a_i(q)$ of the different types of particles found by analyzing the DLS data with the dynamic model. The following specific assumptions were made in the analysis of the amplitudes $a_i(q)$: For the micelles a form factor of monodisperse spheres was assumed (for the micelles the effect of polydispersity is negligible, and $P(q) \approx 1$ in the entire q range). For the fiber aggregates a form factor for cylinders with a Schulz−Zimm distribution for the cylinder length is used. And finally the cluster scattering contribution was described by a form factor of polydisperse spheres.

Analysis of the Amplitudes $a_i(q)$. As a second consistency test of the present model we can take the q dependence of the amplitudes $a(q)_{micelle}$ and $a(q)_{cluster}$. As we have set $a(q)_{fiber}$ to 1 during the fit of $g_2(\tau)$, the amplitudes $a(q)_{micelle}$ and $a(q)_{cluster}$ are given by the ratio of the respective weighted static form factors

$$a_i(q) = \frac{A_i P(q)_{sphere,poly}}{P(q)_{fiber,cylinder}} \qquad (8)$$

with the relative static amplitude A_i at $q = 0$

$$A_i = \frac{A_i^0}{A_{fiber}^0} \qquad (9)$$

Here, $P(q)_{sphere,poly}$ is the form factor of homogeneous spheres with a Gaussian distribution of the sphere radius.[48] $P(q)_{fiber,cylinder}$ is the form factor of a homoge-

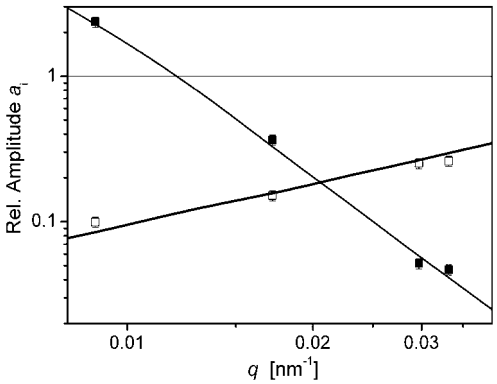

Figure 6. Relative amplitudes $a_i(q)$ as a function of q for micelles (open symbols) and cluster aggregates (dark symbols). The lines represent the modeled q dependence according to eq 8. The amplitudes are expressed relative to the amplitude of the fiber aggregates.

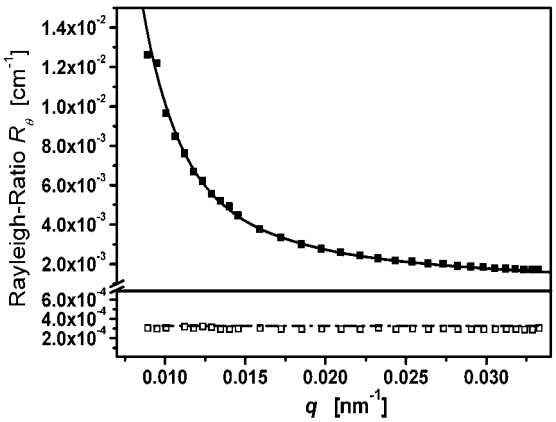

Figure 7. Top: measured total static intensity $R(q)$ (dark squares) and model curve according to eq 10 (solid line) for sample H3; bottom: measured static intensity $R(q)$ for a pure C_8E_4 solution (open squares) and the micellar contribution A^0_{micelle} from the model (dash−dotted line).

neous cylinder with a Schulz−Zimm distribution of length L_w.[48] The cross-sectional diameter d is of no importance in the q interval probed in LS. The fit of eq 8 to the $a_i(q)$ reveals the relative static amplitudes A_i of the micelles and clusters at $q = 0$.

Figure 6 displays the relative amplitudes $a_i(q)$ from the DLS data analysis and modeled by eq 8 for sample H3. The model for the analysis of the static light scattering data qualitatively predicts the relative amplitudes obtained from the DLS experiments. This is an additional proof for the correctness of the used approach.

Analysis of the Rayleigh Ratio $R(q)$. With the information about the ratio of the three contributions to the static scattering intensity, we can apply the sum of the form factors to the measured $R(q)$. Equation 6 with relative amplitudes (eq 9) reads

$$R(q) = A^0_F(P(q)_{\text{cyli}} + A_C P(q)_{\text{sphere}} + A_M P(q)_{\text{sphere}}) \tag{10}$$

Note that the only parameters adjusted in eq 10 during the fit are the static amplitude A^0_{fiber}, the polydispersity for the cluster radius, and the polydispersity for the fiber length L_c. All other parameters are taken from the dynamic light scattering data analysis. In Figure 7 the measured $R(q)$ for sample H3 and in Figure 8 for sample series K are shown in dependence on q. The measured q dependence is very well described by the relative static

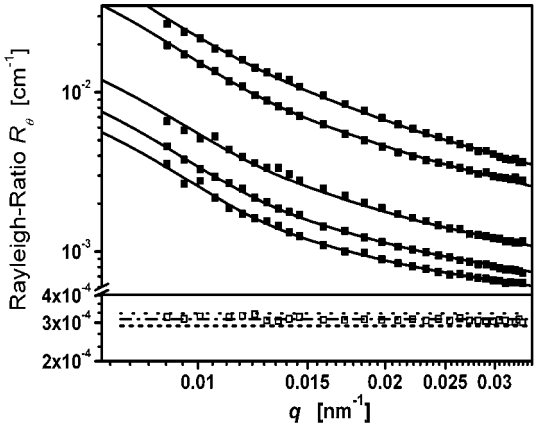

Figure 8. Top: measured total static intensity $R(q)$ (dark squares) and model curves according to eq 10 (solid lines) for samples K1−K5 (from lowest to topmost curve); bottom: measured static intensity $R(q)$ for a pure C_8E_4 solution (open squares) and the micellar contributions A^0_{micelle} from the model (dashed lines).

amplitudes A_i from the DLS data analysis. The found static amplitudes A^0_{fiber} are listed in Table 3. For the cluster radius values for the polydispersity of 18−25% are found from the SLS data analysis. For the polydispersity of the fiber length L_c values for the polydispersity parameter k of $1.2 < k < 1.8$ are found, which is in qualitative agreement with the values found for the DLS data analysis. With the mass concentration c of the fiber aggregates and the respective contrast factor K the apparent molar mass of the fiber aggregates is calculated and listed in Table 3. From the apparent molar mass $M_{w,\text{fiber}}$ and the averaged length L_w from the DLS analysis the linear mass density M_w/L_w of the fiber aggregates can be calculated. The length of a monomer unit of PPP(12) along the fiber axis is known (0.42 nm),[21] and thus the apparent radial aggregation number $N_{\text{rad,app}}$ can be determined. The calculated averaged length L_w and the calculated values of $N_{\text{rad,app}}$ are listed in Table 3, too. The values of $N_{\text{rad,app}}$ show no significant concentration dependence and are similar for both sample series (H and K). The found value $N_{\text{rad}} = 21$ is in rather good agreement with $N_{\text{rad}} = 16$ found by Bockstaller and co-workers for the PPP-sulfonates in aqueous solution.[11,12] The lower value of 16 can be explained by the repulsive interaction of the anionic sulfonate headgroups and the lower alkyl chain density in the core of their fiber aggregates. In the case of the PPP-sulfonate, only every third benzene ring is substituted with a dodecyl alkyl chain. Both effects result in a higher curvature and thus in a reduced cross-sectional radius of the fiber aggregates, i.e., a lower value of N_{rad}.

Besides the static amplitudes A^0_{fiber}, the static amplitudes A^0_{micelle} are known from the SLS data analysis (see eq 9). These values can be compared to the respective value for a pure C_8E_4/H_2O solution. This comparison is shown in the lower part of Figure 7 for sample H3 and of Figure 8 for sample series K. In all cases, the static amplitudes from the data analysis fit well to the directly measured static intensity $R(q)_{\text{micelle}}$. This is again a good verification for the consistency of the applied data analysis procedure for the DLS and SLS data. (Note that the accuracy of $R(q)_{\text{micelle}}$ is not sufficient to determine the amount of C_8E_4 incorporated into the fiber aggregates. This is done with SANS (see ref 26).) For the systems PPP(12) in $C_{12}E_6/H_2O$ and in $C_{10}G_2/H_2O$ the found values for A^0_{fiber}, L_w, and $N_{\text{rad,app}}$

Table 3. Static Amplitudes A^0_{fiber} at $q = 0$ from Applying Eq 10 to $R(q)$, the Used Concentrations of the Fiber Aggregates c_{fiber} To Calculate the Apparent Molar Mass $M_{w,app}$ of the Fiber Aggregates, and the Weight-Averaged Length L_w from the DLS Analysis Used To Calculate the Apparent Radial Aggregation Number $N_{rad,app}$

	$A^0_{fiber} \times 10^{-3}$ [cm^{-1}] SLS	c_{fiber}[a] [mg/g]	$M_{w,app} \times 10^6$ [g/mol]	L_w [nm] DLS	$N_{rad,app}$
series H					
1	3.3 ± 0.1	0.62	16 ± 2	680 ± 70	23 ± 6
2	5.6 ± 0.1	1.20	14 ± 2	580 ± 60	24 ± 7
3	11.4 ± 0.3	2.52	14 ± 2	720 ± 70	18 ± 5
4	44.1 ± 0.4	4.92	25 ± 2	1090 ± 110	23 ± 4
series K					
1	1.7 ± 0.1	0.62	8 ± 2	410 ± 40	19 ± 7
2	2.5 ± 0.1	0.96	8 ± 2	440 ± 40	18 ± 6
3	7.0 ± 0.2	1.25	17 ± 2	700 ± 70	24 ± 5
4	27.0 ± 0.3	3.84	20 ± 2	960 ± 90	21 ± 4
5	41.9 ± 0.4	5.13	25 ± 2	1190 ± 120	21 ± 3
in $C_{12}E_6/H_2O$					
	11.5 ± 0.3	4.0	9 ± 2	580 ± 60	16 ± 4
in $C_{10}G_2/H_2O$					
	13.0 ± 0.4	3.6	9 ± 2	490 ± 50	17 ± 5

[a] An amount of 20 wt % of the fiber aggregates is assumed to be the surfactant C_8E_4 to calculate c_{fiber} (see ref 26 polymer-to-surfactant ratio).

are listed in Table 3, too. As already found in the DLS data analysis, the values are of the same order of magnitude compared to the PPP(12)/C_8E_4/H_2O system.

V. Conclusion

We have studied the aggregation of an amphiphilic 2,5-disubstituted poly(*p*-phenylene) in micellar surfactant solutions by a combination of static and dynamic light scattering techniques. This mixed polymer−surfactant system contains distinctly different particles, and the focus of the present article has been on methods to derive structural information about one of these particles in the presence of an excess of other particles also exhibiting mesoscopic dimensions.

Cryo-TEM images of mixed aqueous solutions of the polymer PPP(12) and a nonionic surfactant (C_8E_4 or $C_{12}E_6$) indicate the existence of elongated and stiff (fiberlike) aggregates of a contour length $L > 200$ nm and a cross-sectional diameter of ca. 6 nm in the presence of an excess of pure surfactant micelles. The dynamic behavior of this system was studied by dynamic light scattering. The measured intensity autocorrelation function comprises three contributions, which can be attributed to the surfactant micelles, the fiber aggregates, and an even larger entity, the nature of which is not yet totally clear. From the observation that the hydrodynamic radius R_H of these entities increases with increasing polymer concentration, it is proposed that these particles may represent clusters of fiber aggregates, as known from polyelectrolyte type poly(*p*-phenylene) sulfonates[11,12] below the isotropic−nematic phase transition. The critical concentration c_{crit} of this isotropic−nematic phase transition can be estimated on the basis of the Onsager theory[13] for stiff rods in solution, which yields $c_{crit} \approx 7$ g/kg for the present fiber aggregates. Accordingly, the conjectured formation of clusters and the absence of a nematic phase is consistent with the prediction of the Onsager theory, as in our study the highest polymer concentration was below 7 g/kg.

The contribution of the fiber aggregates to the DLS intensity autocorrelation function was analyzed in terms of a dynamic model of stiff rods, which shows that the number-averaged length L_n, which is about 300−800 nm, scales with the polymer concentration according to the power law $L \propto c^{0.5}$, as known for "living polymers" (e.g., $C_{12}E_5$ in H_2O).[16] The polydispersity of the length L can be represented by a Schulz−Zimm distribution. On the basis of these results a static model is presented, which describes the q dependence of the relative amplitudes from the dynamic light scattering data as well as the Raleigh ratio $R(q)$ from static light scattering. This combined analysis of the DLS and SLS data leads to the molar mass M_w of the fiber aggregates und thus to the radial aggregation number $N_{rad} \approx 21$.

The great length of the stiff fiber aggregates hints at a lengthwise arrangement of the PPP backbones along the fiber long axis. Thus, the present PPP(12)/surfactant/water system represents a first example for an uncharged poly(*p*-phenylene), exhibiting a lengthwise aggregation of quasi-stiff molecules in selective solvents.

In conclusion, we have discussed strategies how light scattering techniques can be used to determine properties of elongated fiber aggregates in the presence of other scattering particles. Although the models used in the analysis are specific for the present system, most of the strategies can be adapted to account for other types of complex mixed systems as well.

The internal structure of the aggregates will be discussed in the second paper of this study.[26]

Acknowledgment. Financial support from the Deutsche Forschungsgemeinschaft (DFG) through SFB 448, and complementary support through the Fonds der Chemischen Industrie, is also gratefully acknowledged.

References and Notes

(1) Kranzelbinder, G.; Byrne, H. J.; Hallstein, S.; Roth, S.; Leising, G.; Scherf, U. *Phys. Rev. B* **1997**, *56*, 1632−1636.
(2) Savvateev, V. N.; Yakimov, A.; Davidov, D. *Adv. Mater.* **1999**, *11*, 519−531.
(3) Grice, A. W.; Bradley, D. D. C.; Bernius, M. T.; Inbasekaran, M.; Wu, W. W.; Woo, E. P. *Appl. Phys. Lett.* **1998**, *73*, 629−631.
(4) Harrison, B. S.; Foley, T. J.; Bouguettaya, M.; Boncella, J. M.; Reynolds, J. R.; Schanze, K. S.; Shim, J.; Holloway, P. H.; Padmanaban, G.; Ramakrishnan, S. *Appl. Phys. Lett.* **2001**, *79*, 3770−3772.
(5) Pan, J.; Scherf, U.; Schreiber, A.; Haarer, D. *J. Chem. Phys.* **2000**, *112*, 4305−4309.
(6) Neher, D. *Adv. Mater.* **1995**, *7*, 691−702.
(7) Bo, Z.; Zhang, Ch.; Severin, N.; Rabe, J. P.; Schlüter, A. D. *Macromolecules* **2000**, *33*, 2688−2694.
(8) Engelking, J.; Wittmann, M.; Rehahn, M.; Menzel, H. *Langmuir* **2000**, *16*, 3407−3413.
(9) Bo, Z.; Rabe, J. P.; Schlüter, A. D. *Angew. Chem., Int. Ed.* **1999**, *38*, 2370−2372.

(10) Liu, T.; Rulkens, R.; Wegner, G.; Chu, B. *Macromolecules* **1998**, *31*, 6119−6128.
(11) Bockstaller, M.; Köhler, W.; Wegner, G.; Fytas, G. *Macromolecules* **2001**, *34*, 6353−6358.
(12) Bockstaller, M.; Köhler, W.; Wegner, Vlassopoulos, D.; G.; Fytas, G.; *Macromolecules* **2001**, *34*, 6359−6366.
(13) Onsager, L. *Ann. N.Y. Acad. Sci.* **1949**, *51*, 627−659.
(14) Israelachvili, J. *Intermolecular and Surface Forces*, 2nd ed.; Academic Press: London, 1991; Chapter 17.
(15) Cates, M. E. *Macromolecules* **1987**, *20*, 2289−2296.
(16) Menge, U.; Lang, P.; Findenegg, G. H. *Colloids Surf. A* **2000**, *163*, 81−90.
(17) Strey, R. *Curr. Opin. Colloid Interface Sci.* **1996**, *1*, 402−410.
(18) Kahlweit, M.; Strey, R. *Angew. Chem.* **1985**, *97*, 655−669.
(19) Stubenrauch, C. *Curr. Opin. Colloid Interface Sci.* **2001**, *6*, 160−170.
(20) Stubenrauch, C.; Findenegg, G. H. *Langmuir* **1998**, *14*, 6005−6012.
(21) Fütterer, T.; Hellweg, T.; Findenegg, G. H.; Frahn, J.; Schlüter, A. D.; Böttcher, C. *Langmuir* **2003**, *19*, 6537−6544.
(22) Schönfelder, E.; Hoffmann, H. *Ber. Bunsen-Ges. Phys. Chem.* **1994**, *98*, 842−852.
(23) Würtz, J.; Hoffmann, H. *J. Colloid Interface Sci.* **1995**, *175*, 304−317.
(24) Won, Y.-Y.; Brannan, A. K.; Davis, H. T.; Bates, F. S. *J. Phys. Chem. B* **2002**, *106*, 3354−3364.
(25) Nordskog, A.; Egger, H.; Findenegg, G. H.; Hellweg, T.; Schlaad, H.; Berlepsch, H. v.; Boettcher, C. *Phys. Rev. E* **2003**, *68*, 011406/1−011406/14.
(26) Fütterer, T.; Hellweg, T.; Findenegg, G. H.; Frahn, J.; Schlüter, A. D. *Macromolecules* **2005**, *38*, 7451−7455.
(27) Frahn, J.; Schlüter, A. D. *Synthesis* **1997**, *11*, 1301−1304.
(28) Frahn, J. Ph.D. Thesis, Freie Universität Berlin, Berlin, Germany, 1999.
(29) Schlüter, A. D. *J. Polym. Sci., Part A: Polym. Chem.* **2001**, *39*, 1533−1556.
(30) Strunk, H. Ph.D. Thesis, Technische Universität Berlin, Berlin, Germany, 1995.
(31) Evilevitch, A.; Lobaskin, V.; Olsson, U.; Linse, P.; Schurtenberger, P. *Langmuir* **2001**, *17*, 1043−1053.
(32) Berne, B. J.; Pecora, R. *Dynamic Light Scattering*; John Wiley & Sons: New York, 1976.
(33) Provencher, S. W. *Comput. Phys. Commun.* **1982**, *27*, 213−217.
(34) Provencher, S. W. *Comput. Phys. Commun.* **1982**, *27*, 229−242.
(35) Drögemeier, J.; Hinssen, H.; Eimer, W. *Macromolecules* **1994**, *27*, 87−95.
(36) Lang, P.; Kajiwara, J. K.; Burchard, W. *Macromolecules* **1993**, *26*, 3992−3998.
(37) Zwanzig, R. *Annu. Rev. Phys. Chem.* **1965**, *16*, 67−102.
(38) Russo, P. S. In *Dynamic Light Scattering*; Brown, W., Ed.; Clarendon Press: Oxford, 1993; Chapter 12.
(39) Pecora, R. *J. Chem. Phys.* **1968**, *49*, 1036−1043.
(40) Fütterer, T. Ph.D. Thesis, Technische Universität Berlin, Berlin, Germany, 2004.
(41) Doi, M.; Edwards, S. F. *The Theory of Polymer Dynamics*; Oxford University Press: Oxford, 1986; Chapter 7.
(42) Broersma, S. *J. Chem. Phys.* **1960**, *32*, 1626−1631.
(43) Broersma, S. *J. Chem. Phys.* **1960**, *32*, 1632−1635.
(44) Hellweg, T.; Eimer, W.; Krahn, E.; Schneider, K.; Müller, A. *Biochim. Biophys. Acta* **1997**, *1337*, 311−318.
(45) Lösche, M.; Schmitt, J.; Decher, G.; Bouwman, W. G.; Kjaer, K. *Macromolecules* **1998**, *31*, 8893−8906.
(46) Fütterer, T.; Hellweg, T.; Findenegg, G. H. In *Mesoscale Phenomena in Fluid Systems*; Case, F., Alexandridis, P., Eds.; ACS Symposium Series 861; American Chemical Society: Washington, DC, 2003; Chapter 8.
(47) Bender, T. M.; Lewis, R. J.; Pecora, R. *Macromolecules* **1986**, *19*, 244−245.
(48) Pedersen, J. S. *Adv. Colloid Interface Sci.* **1997**, *70*, 171−210.

MA050318H